Scientific Research Publishing

Open Journal of Medical Imaging, 2023, 13, 11-29
https://www.scirp.org/journal/ojmi
ISSN Online: 2164-2796
ISSN Print: 2164-2788

Quality Assuring a Ring Vortex Flow Phantom in Real-Time

Alana S. Matthews[1,2*], Kelvin Simatwo[2,3], Andrew Narracott[1,2], Simone Ambrogio[4], Adrian Walker[5], John W. Fenner[1,2]

[1]Department of Infection, Immunity and Cardiovascular Disease, Mathematical Modelling in Medicine Group, University of Sheffield, Sheffield, UK
[2]Insigneo Institute for In Silico Medicine, University of Sheffield, Sheffield, UK
[3]Department of Electronic and Electrical Engineering, University of Sheffield, Sheffield, UK
[4]Medical Physics Department, Guy's and St Thomas' NHS Foundation Trust, London, UK
[5]Leeds Test Objects, Boroughbridge, UK

Email: *asmatthews2@sheffield.ac.uk

How to cite this paper: Matthews, A.S., Simatwo, K., Narracott, A., Ambrogio, S., Walker, A. and Fenner, J.W. (2023) Quality Assuring a Ring Vortex Flow Phantom in Real-Time. *Open Journal of Medical Imaging*, **13**, 11-29.
https://doi.org/10.4236/ojmi.2023.131002

Received: November 30, 2022
Accepted: March 3, 2023
Published: March 6, 2023

Abstract

Introduction: The ring vortex phantom is a novel, cost-effective prototype which generates complex and well-characterised reference flows in the form of the ring vortex. Although its reproducibility has been demonstrated, with ring speeds routinely behaving within 10% tolerances at speeds of approximately 10 - 70 cm/s, a form of real-time QA of the device at the time of imaging is needed to confirm correct function on demand in any environment. **Methods:** The technology described here achieves real-time QA, comprising a linear encoder, laser-photodiode array, and Doppler probe, measuring piston motion, ring speed and intra-ring velocity respectively. This instrumentation does not interfere with imaging system QA, but allows QA to be performed on both the ring vortex and the device in real-time. **Results:** The encoder reports the reliability of the piston velocity profile, whilst ring speed is measured by laser behaviour. Incorporation of a calibrated Doppler probe offers a consistency check that confirms behaviour of the central axial flow. For purposes of gold-standard measurement, all elements can be related to previous Laser PIV acquisitions with the same device settings. **Conclusion:** Consequently, ring vortex production within tolerances is confirmed by this instrumentation, delivering accurate QA in real-time. This implementation offers a phantom QA procedure that exceeds anything seen in the literature, providing the technology to enhance quantitative assessment of flow imaging modalities.

Keywords

Flow Phantom, Ring Vortex, Quality Assurance, Imaging

1. Introduction

The development of complex flow phantoms is increasingly important due to the rise of quantitative flow imaging technologies capable of visualising physiological fluid behaviour in detail. State-of-the-art modalities such as 4D-MRI and Vector Flow Imaging (VFI) are being refined for widespread use both in the clinic and research. 4D-MRI has demonstrated its ability to calculate quantitative information previously unachievable [1], whilst VFI has exhibited strong correlation with traditional MRA [2] and is capable of quantitatively visualising complex flow to high resolution [3]. Imaging data from these modalities are often in the form of quantitative vector flow fields, which is a significant advancement over traditional medical imaging outputs, and allows for more thorough haemodynamic analysis. With the improved visualisation capabilities of these technologies, flow phantoms should ideally generate flows with 1) sufficiently complex flows to challenge the modalities, and 2) well-characterised behaviour at both bulk and sub-mm (*i.e.* "micro") scales.

The ring vortex flow phantom has been developed to generate such flows, producing reproducible ring vortices over a range of speeds and sizes [4]. Reproducibility is vital for application as a medical flow phantom, and its reference flows have also been demonstrated as predictable, controllable and stable [5]. In addition to these attributes, the complexity of the ring vortex flow is sufficiently demanding to challenge modern flow imaging systems, with flow features directly relevant to intra-cardiac flow profiles [6]. The ring vortex phantom in its current incarnation (as manufactured by Leeds Test Objects) is suited for use with ultrasound and CT-based imaging modalities, and has demonstrated rings with measurable, reproducible bulk behaviour in terms of ring speed and size to within 10% tolerances in a laboratory setting. There is concern however that in less controlled environments, tolerances might exceed the stated bounds and that such flows are difficult to validate. This is an important criticism since phantoms are required to reliably provide an accurate "ground truth" reference by which to judge imaging performance.

This paper describes methodology that independently confirms the quality of each ring during vortex ring propagation using dedicated instrumentation. The result is a real-time, capable of assessing imaging system performance while simultaneously providing real-time device QA and flow QA measurements to confirm correct production of the ring vortex flow. The methods section below provides details of phantom instrumentation and describes operational requirements, whilst the Results section reports the effectiveness of this approach. The discussion explores comparison to other works and considers implication for future application.

2. Ring Vortex Characterisation

Ring vortex behaviour is discussed broadly in the literature, with Didden [7] offering quantifiable metrics, identifying that the ring vortex can be usefully cha-

racterised by ring diameter, core diameter, circulation and ring translational speed (see **Figure 1**). The ring is formed primarily of a torus of recirculating fluid layers, surrounded by a volume of fluid which propagates with the ring, known as the vortex atmosphere [8]. These metrics are heavily dependent on the generating conditions of orifice diameter, piston velocity profile and displacement, and fluid viscosity.

A method widely used for characterizing ring vortex behaviour is video acquisition, previously used with the ring vortex phantom. Rings are visualised with liquid dye or smoke, and their paths recorded and subsequently analysed in post-processing [8] [9] [10]. The method allows for bulk characterisation, with vortex size and ring speed measured. The addition of Laser Doppler velocimetry (LDV) offers micro-characterisation at the sub-mm scale, enabling velocities to be determined at specific points within the flow field. Ring vortex characterisation using LDV is evident in the literature [11] [12].

Increased computational power has inspired particle imaging velocimetry (PIV), an optical method that achieves vector visualisation of the flow in a short timeframe. Its results agree with LDV measurements [13], and are used often for high-resolution fluid visualisation. Its application to ring vortices is broad, with both vortex formation [14] [15] and evolution [16] [17] [18] [19] imaged extensively. PIV is a powerful tool which, when combined with analysis techniques such as streamline generation (**Figure 2(b)**) or Lagrangian structures, can provide rich information concerning the intricacies of the vortex flow field. Details of PIV methodology are given below, in Methods.

However, none of the above (video, LDV, PIV) can be considered real-time since they require significant processing to quantify flow characteristics following data acquisition. The requirement for specialised equipment typically in a lab setting also restricts broader application of LDV and PIV. Despite this, the richness

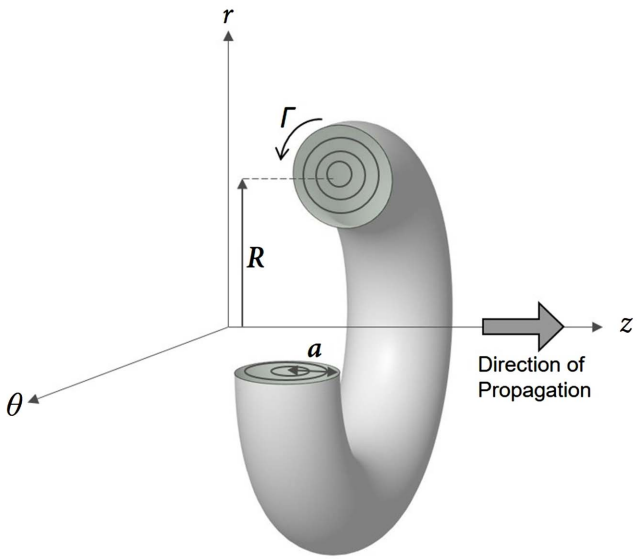

Figure 1. A schematic of the ring vortex with cylindrical coordinate system. Core radius (a, mm), ring radius (R, mm and circulation (Γ, $mm^2 \cdot s^{-1}$) are noted.

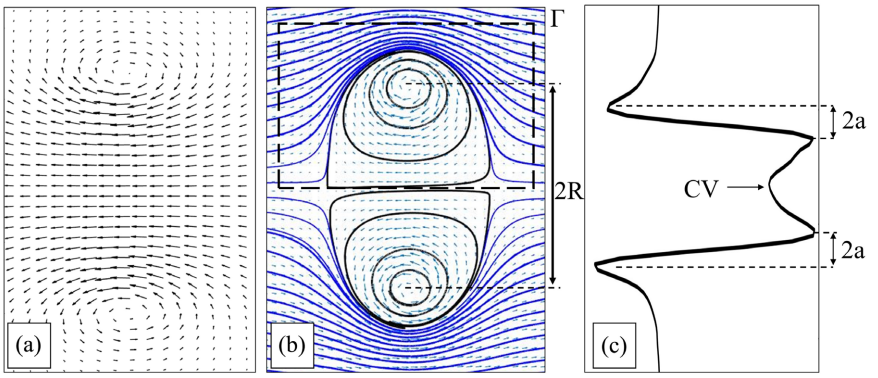

Figure 2. Example Laser PIV data from the ring vortex phantom. (a) Raw velocity vector profile. (b) Annotated vector plot with streamlines, ring radius and circulation denoted. (c) Projection of axial velocities vertically down the ring centre. Core diameter (2a), ring diameter (2R) and CentVect (C.V.) are noted.

of the processed data allows for direct measurement of the vortex properties as presented by Didden. An example from the ring vortex phantom is seen in **Figure 2**, where ring diameter, core diameter and circulation can be extracted from the measured PIV flow field.

Ring diameter is the distance between core centres (defined by the point of maximum absolute vorticity). Core diameter is often reported as either the distance between maximum and minimum tangential velocity [20] or the distance between 10% of the maximum vorticity [21]. In this paper, the former, velocity-derived method is used, with the radius taken as the average of axial and radial measurements from both cores. Circulation is measured by computing a line integral of the velocity vectors around a domain centred at the vortex core. Finally, ring speed can be determined by calculating the ring displacement between adjacent frames and dividing by the elapsed time. Vortex atmosphere dimensions can also be derived from streamlines; however, this characteristic is not reported in this work.

With these straightforward measurements, ring vortex characterisation is possible and can be capably delivered by PIV, arguably providing a gold standard reference that represents the ultimate in ring QA. On the other hand, PIV is not viable as a routine tool for clinical imaging systems; because of its expense, the requirement for specialist setup with intricate optical alignment, and inability to perform real-time measurements—datasets must be processed after data collection to characterise vortices. Arguably any alternative to quality assuring the ring should endeavour to be consistent with PIV. For the ring vortex phantom discussed in this paper, the primary objective is to ensure that each ring vortex generated exhibits behaviour that is within tolerances (e.g. +/−10%) in relation to the PIV gold standard. The methods for real time QA reported here employ a linear encoder, laser scattering and a Doppler probe.

3. Methods

This section describes the methods implemented to achieve PIV-consistent QA.

First the ring vortex generating conditions are described, then the Laser PIV methodology followed by a description of the instrumentation.

3.1. Ring Vortex Generation

To demonstrate real time QA of the ring vortex flows, a selection of ring vortices was generated, covering a range of generating conditions. Ten rings of each configuration (Table 1) were produced, and their defining characteristics determined by the three methods (linear encoder, laser scattering and Doppler probe), each of which was referenced to the PIV gold standard.

Rings were generated using the well-established piston-orifice setup used by the ring vortex phantom. Figure 3 illustrates that the piston is driven by a bipolar

Table 1. Table type styles (Table caption is indispensable).

Config	Orifice Diameter	Max Piston Speed	Programmed Piston Displacement	Re	PIV Speed Reproducibility
1	10 mm	5.3 ± 0.3 cm/s	0.8 mm	13,028	12%
2	10 mm	4.2 ± 0.3 cm/s	0.8 mm	11,166	4.6%
3	15 mm	5.3 ± 0.3 cm/s	0.8 mm	8674	7.6%
4	15 mm	4.2 ± 0.3 cm/s	0.8 mm	7434	16%
5	20 mm	5.3 ± 0.3 cm/s	0.8 mm	6514	5.8%
6	20 mm	4.2 ± 0.3 cm/s	0.8 mm	5583	30%

The generating conditions applied for validation of the real-time ring vortex quality assurance tool.

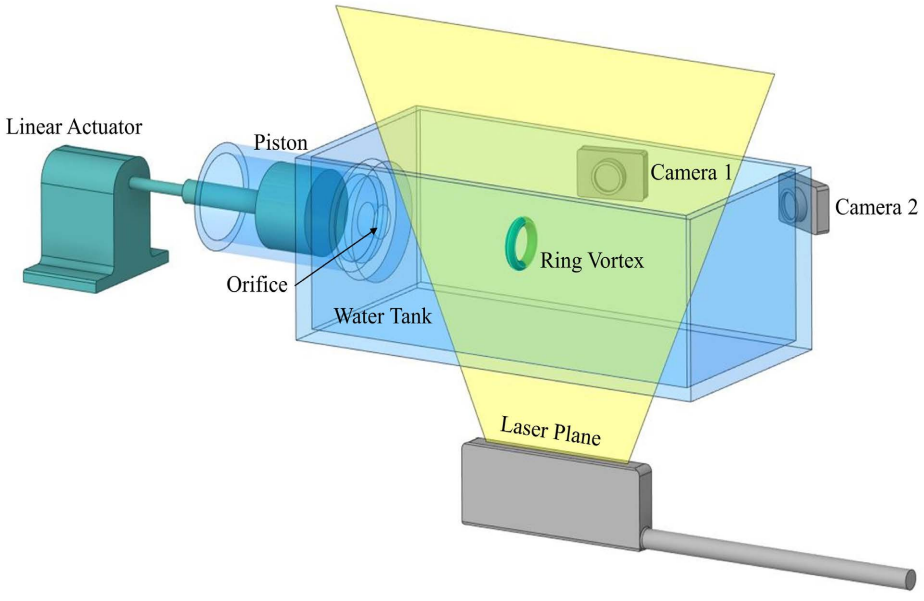

Figure 3. A schematic of the ring vortex phantom with Laser PIV equipment. The linear actuator propels a piston, thus ejecting a slug of fluid through the orifice. This generates a ring vortex propagating through the tank. This tank is bisected by a laser projected from below, with stereoscopic cameras capturing particle motion in three dimensions.

stepper motor, which is user-controlled via an Arduino Uno microcontroller. The piston speed and displacement can be dictated by the user, and the orifice size (10 mm, 15 mm, 20 mm, 25 mm are available) selected. The largest orifice was not used in this exercise, as its rings are known to be unreliable and unstable [4]. Rings were generated at 25 s intervals to allow the ambient fluid volume to settle between ring propagation. Characteristics were recorded using the instrumentation described below. It is worth noting here that configurations 1, 4 and 6 exceeded the ideal tolerance of 10%, removing them from contention as reference flows. In future work, configurations will be refined to ensure all exhibit ideal tolerances.

3.2. Laser PIV

The laser PIV (the gold-standard datasets for this device) enabled characteristic parameters (ring speed, dimensions and intra-ring flow velocities) to be obtained. Ring vortex behaviour was captured over a horizontal distance 9 - 23 cm from the orifice, requiring a low concentration of 10 - 20 mm diameter, neutrally buoyant, fluorescent nylon particles to be mixed throughout the fluid volume, complemented by a double-pulse laser positioned below the tank. A laser sheet was projected vertically along the tank axis, (see **Figure 3**) cutting the rings through their centre. The use of stereoscopic cameras captured particle displacement in consecutive frames, with correlation techniques used to produce high-accuracy (<+/−0.1% declared by LaVision UK) velocity vector maps of the ring vortex in cross-section (see **Figure 2**). Spatial and temporal resolution were 0.8 mm and 71.4 ms respectively. For a more thorough description, see Ambrogio *et al.* (2019) [4]. Analysis of this data offers full characterisation of the vortex flow at the scale of bulk flow and sub-mm resolution.

3.3. Real-Time QA Instrumentation

PIV offers thorough characterisation of bulk and micro-flow after post-experiment analysis, whereas introduction of strategic instrumentation enables measurement of device and flow performance in real-time. The chosen elements—linear encoder (device QA), laser-photodiode array (flow QA) and a 1D Doppler probe (flow QA)—were used to measure piston impulse, ring speed and a flow-vector component of the micro-flow respectively (**Figure 4**).

3.4. Linear Encoder (Device QA)

The incremental linear encoder (LM10 Incremental Encoder, RLS, Slovenia) monitors phantom function ("device QA"). Circulation of the ring vortex flow can be inferred from piston motion, but in this exercise the encoder measurements were used only to monitor piston performance. The encoder was attached to the piston guide adjacent to a 10 cm long magnetic strip embedded in the piston stem. The ring vortex is generated as the piston is propelled towards the orifice, with the encoder tracking piston motion and recording the displacement/time profile as it moves. Spatial and temporal resolution equated

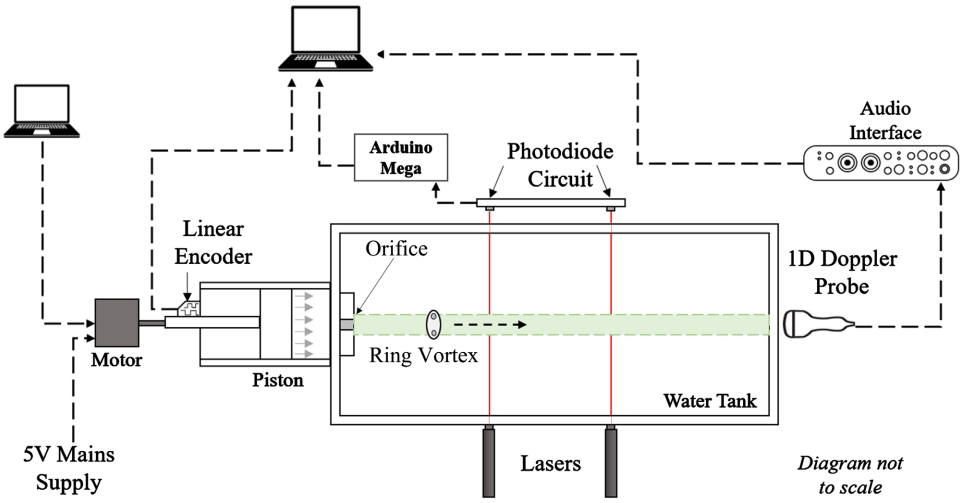

Figure 4. A schematic of the ring vortex phantom, including instrumentation for real-time ring QA. Components are labelled, and dashed arrows represent data/power transfer.

to 10 μm and 1 ms respectively. Reproducibility of piston motion ensures predictability of ring vortex flows.

3.5. Laser Array (Flow QA)

Accurate measurement of bulk ring speed is vital in characterizing the flow, as this often provides the first indication of abnormal ring behaviour. This measurement was achieved through a set of two parallel laser beams of wavelength 500 nm (2 mm diameter beam, continuous, Class 3B) projected across the tank perpendicular to the ring path, positioned to intersect the ring at distances of 8 cm and 18 cm from the orifice. The beams cut the ring through the centre of its path and fall incident on two BPW34 photodiodes on the opposing tank face. These photodiodes are powered and interfaced through an Arduino Mega board [Mega 2560 Rev3, Arduino].

In order for ring capture to be effective, the piston cylinder volume is seeded with absorbing dye and cornflour (concentration ~0.0036 g/ml), which ensure the laser beams are sufficiently attenuated as the ring travels through the beams. Passage of the ring results in a momentary dip in intensity, providing a measurable fluctuation in the photodiode signal. The time difference between the fluctuations is combined with the known laser-to-laser distance to calculate the ring's average speed in the 8 cm - 18 cm interval. Ring propagation was also measured using video acquisition during development to validate this method.

3.6. Doppler Probe (Flow QA)

Finally, a Doppler Probe was used to gain a measure of the micro-flow, based on a 1D 5 MHz continuous wave Hi-Dop Doppler probe (focal length approx. 4 - 8 cm, beam width approx. 5 cm) with the beam axis directed along the axis of travel of the ring. This setup was selected for its straightforward nature and proven ability to measure speeds of scatterers in fluid, providing a measure of the ring

vortex micro-flow along its symmetry axis. Doppler ultrasound is widely used in medical flow imaging, with its application here determining whether intra-ring speeds lie within tolerances. The cornflour-seeded rings produce a high-quality signal, with cornflour used widely in Doppler ultrasound studies [22] [23] [24].

The Doppler probe detects a range of velocities from both translational and rotational motion from within the ring and its surroundings. Within this signal, the axial speed of flow along the central axis of the propagating ring can be extracted, and this measure was designated "CentVect" (see **Figure 2**). CentVect is sensitive to ring energy/circulation, ring radius and core radius and is a critical parameter in respect of the ring vortex. Rather than measuring CentVect directly, the Doppler probe enables consistency checks to be undertaken by virtue of the recorded frequency spectrum. To clarify CentVect, the probe is mounted at the centre of the tank wall facing the orifice, positioned to ensure the beam is directed down the centre of the rings. Although the ring will propagate through the sample volume, with signal frequencies reflecting all micro-speeds in and around the ring. The ultrasound beam width is typically larger than the ring, but appropriate frequency analysis can highlight anomalous frequencies that are not consistent with the PIV standard (**Figure 5**). Evaluating this throughout the ring's journey improves confidence. Incorporating such assessment into the instrumentation generates confidence of consistent ring behaviour at the micro-scale, in addition to the bulk and device measurements described above.

3.7. User Interface

This instrumentation is controlled via a single laptop, using a custom in-house MATLAB application. The lasers, Doppler probe and encoder take readings and compute the ring speed, CentVect and velocity profile in unison, with the results and raw data displayed in an interactive user interface to allow the user to inspect the ring behaviour. This is displayed in **Figure 6**. On-screen indicators

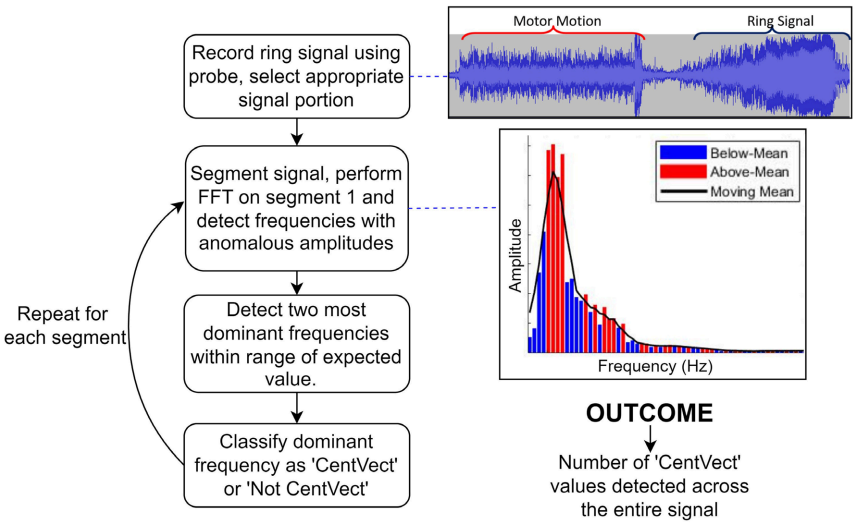

Figure 5. A flowchart depicting the post-processing method used to infer CentVect from the Doppler probe data for the ring vortex.

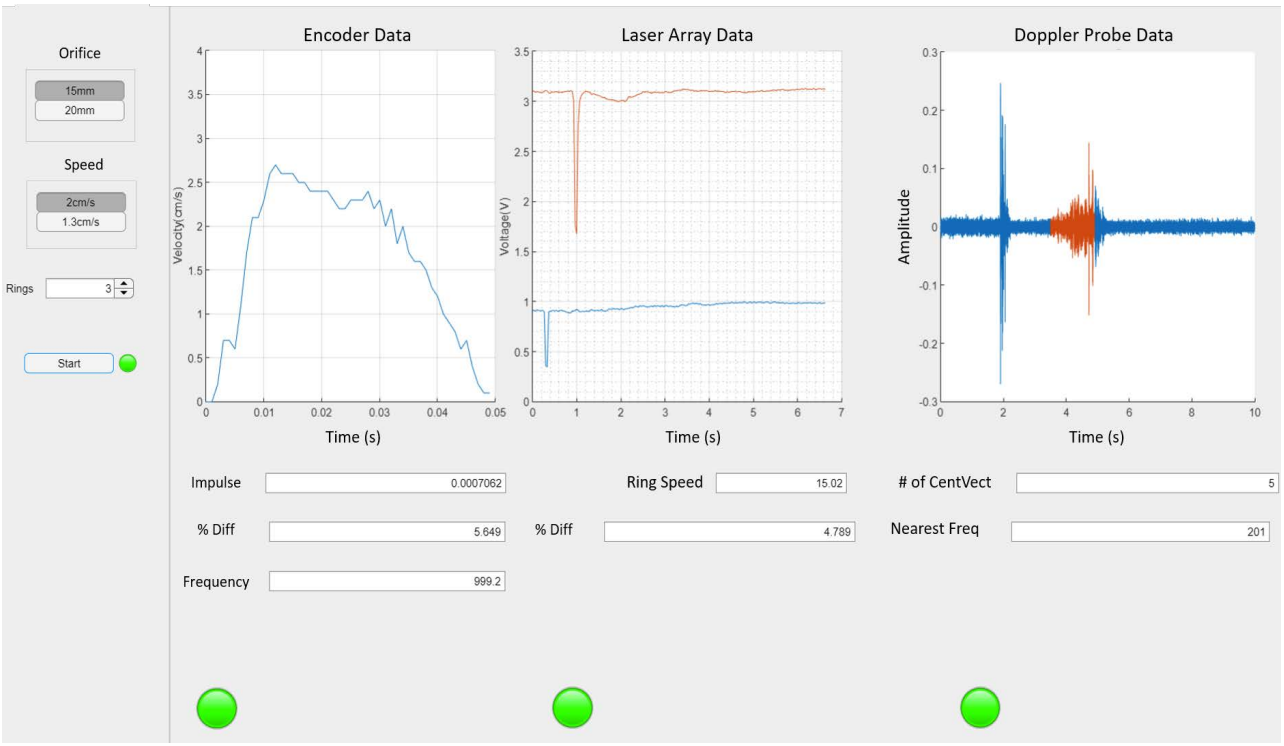

Figure 6. The user interface depicting the raw data outputs of the ring vortex phantom instrumentation pack. The primary calculated measurements (impulse, ring speed and CentVect) are presented, with the corresponding percentage deviation from averaged measurements. The left hand pane is the selection panel, where the user can select the appropriate orifice diameter, piston speed and number of generated rings.

flash green or red, indicating whether each value is within expected tolerances, given the selected phantom settings.

4. Results

The methods described are designed to characterise the vortex ring as it propagates along the tank length. Characteristics of interest are ring speed, piston impulse and CentVect, with an objective to compare average values and variation between gold-standard and new results. Ring behaviour is dictated by generating conditions as listed in Table 1.

4.1. Linear Encoder Results (Device QA)

The linear encoder provides a measure of device performance and reports the position/time history of the generating piston as it expels fluid through the orifice to generate the ring vortex (see Figure 7). Consequently, this is a QA measure of device performance rather than the flow itself. Unsurprisingly, consistent piston performance is synonymous with consistent ring behaviour. The velocity profile of the piston is fundamental to calculating the impulse responsible for generating each ring, through the use of Equation (1). The orifice then converts linear impulse into rotational fluid circulation. For completeness, the derivation for Equation (1) is included in the appendix.

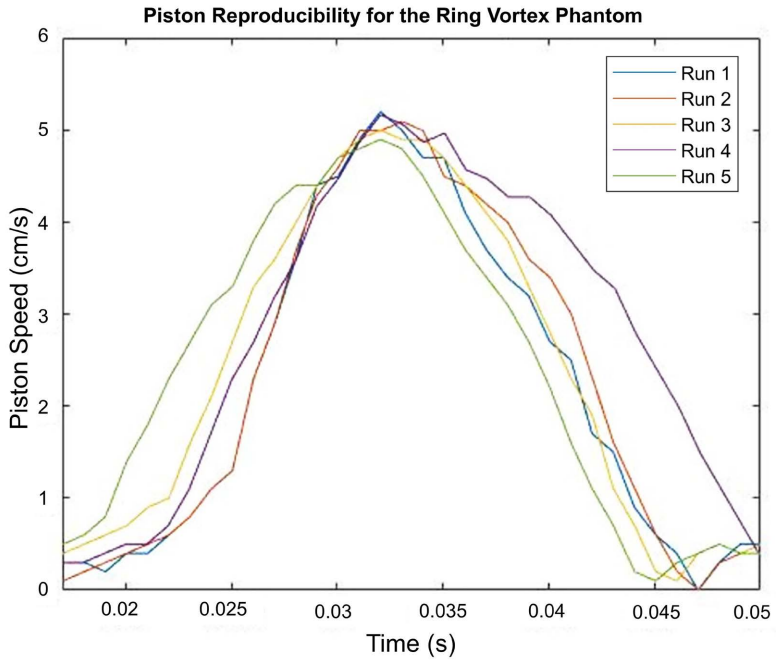

Figure 7. Piston speed as a function of time, responsible for expelling fluid through the orifice to generate the ring vortex. This set of data refers to configuration 1, from which impulse can be calculated and circulation inferred, the latter being responsible for ring speed.

$$I = \frac{\frac{1}{2}\rho\pi R_P^4 L^2}{R_0^2 T} \tag{1}$$

Equation (1) relates encoder motion to impulse (I, N·s) where ρ is fluid density (kg·m^{-3}), R_P is piston diameter (mm), L piston displacement (mm), R_0 orifice diameter (mm) and T time elapsed (s).

Figure 8 illustrates the reproducibility of the piston impulses calculated using Equation 1. Data points represent the average of ten vortex-generating impulses with error bars denoting +/−1SD. Average impulse was deemed the most appropriate measure as it is related to the integral of the velocity profile, thus quantifies both shape and magnitude.

4.2. Laser Scattering Results (Flow QA)

As a direct measure of ring/flow behaviour, Figure 9 demonstrates the correlation between ring translational speed when measured from Laser PIV data and from the laser array method explained above. Each datapoint depicts the average of ten generated rings for the configurations listed in Table 1.

Strong linearity is apparent, and error bars represent +/−1SD. The R^2 value for this dataset is 0.977, with a p-value of 2.06×10^{-2}. When fitted to a linear model, the graph gradient is 1.0205, and the intercept 4.1642, with the near unity gradient confirming the effectiveness of laser measurement to accurately capture ring speed.

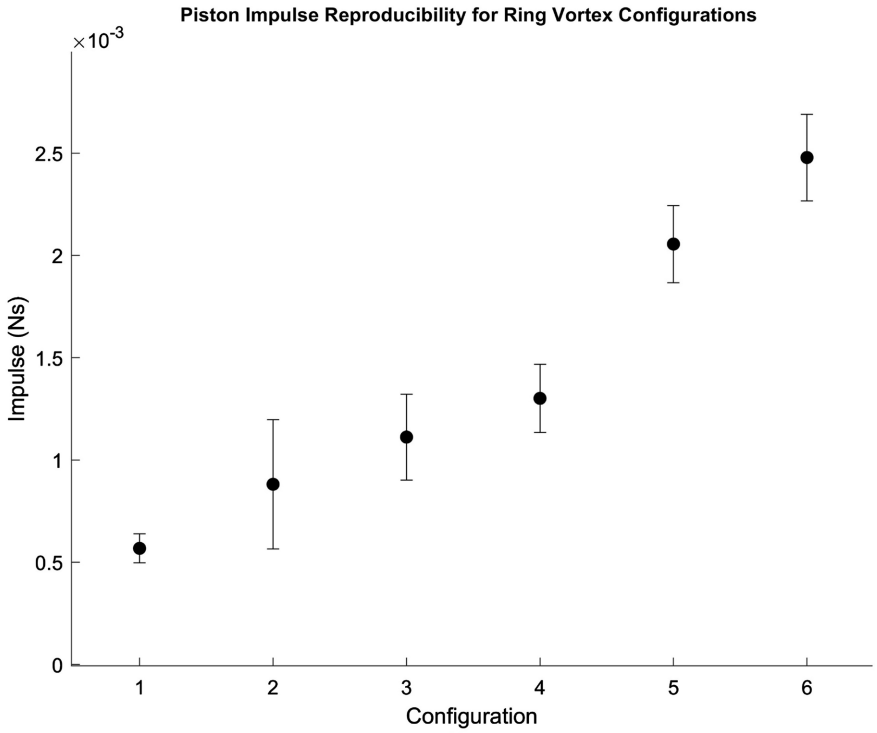

Figure 8. The reproducibility of impulse for configurations 1 - 6, with data collected using the linear encoder. Each datapoint is the average impulse generated by ten piston profiles for that particular configuration. Error bars represent +/−1SD.

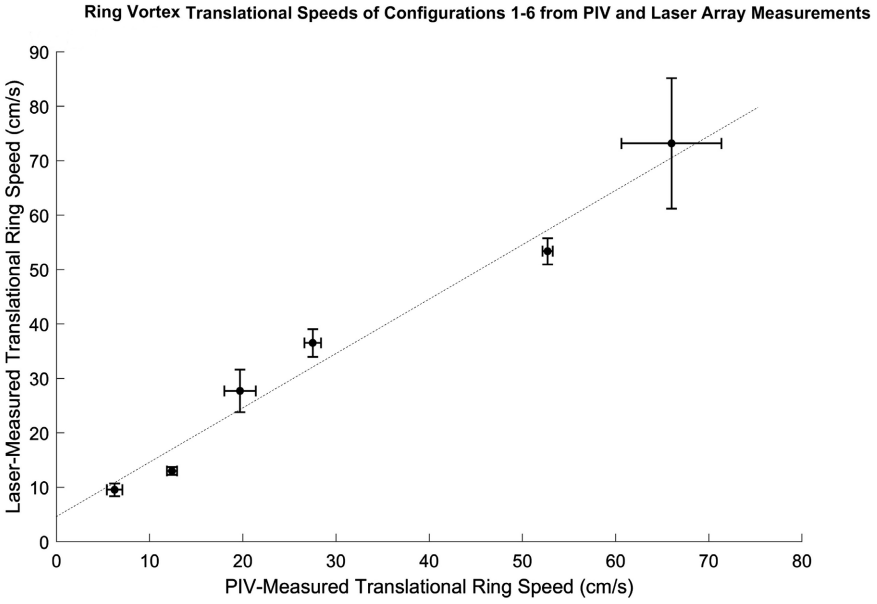

Figure 9. The correlation between PIV-determined ring vortex speeds and Laser-determined ring speeds. Error bars represent +/−1SD.

4.3. Doppler Probe Results (Flow QA)

The Doppler probe also measures ring/flow behaviour, reporting the CentVect parameter of the steadily propagating ring.

Figure 10 demonstrates the strong (and expected) relationship between ring translational speed and CentVect, with both measurements taken using PIV datasets. The R^2 for this correlation is 0.995, and the p-value 1.09×10^{-5}. When fitted to a linear model, its gradient is 2.54 and its intercept −7 cm/s, indicating an offset between the measurements.

The complementary data of Figure 11 presents the correlation between CentVect values from the PIV datasets and values from the Doppler probe signal

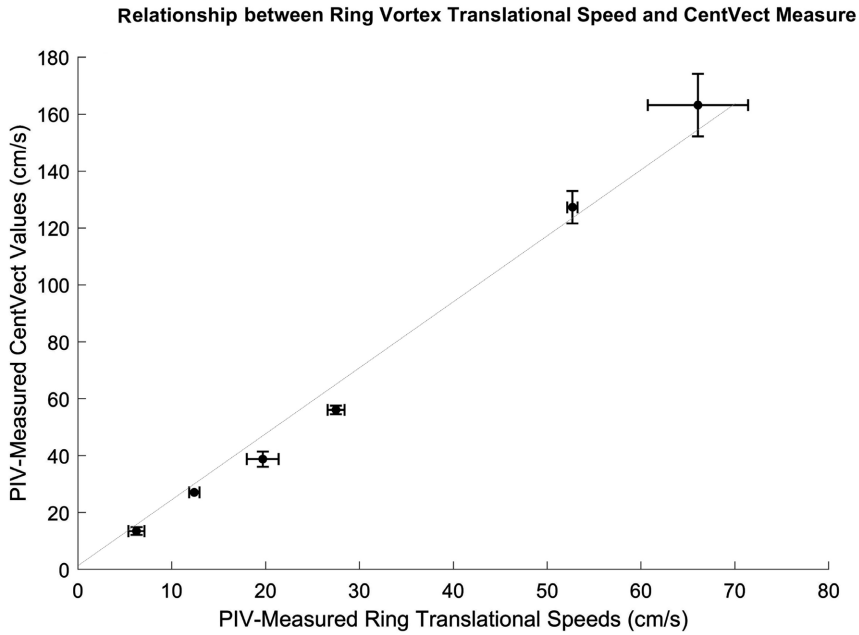

Figure 10. A graph presenting the correlation between ring speed and "CentVect"—the micro-flow measure from the torus' centre. Both measurements are taken from PIV datasets.

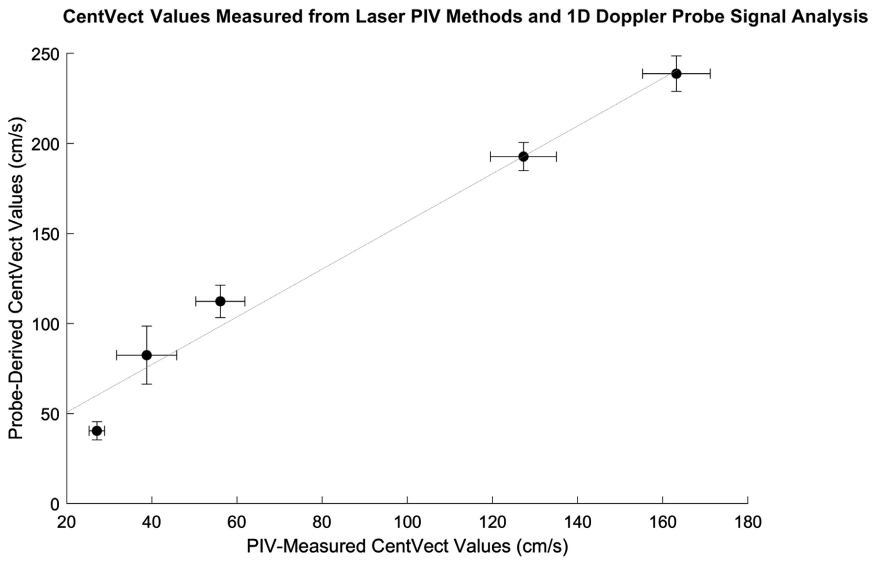

Figure 11. A graph presenting the correlation between CentVect values measured from PIV datasets and those from 1D Doppler probe signal analysis.

analysis, producing a gradient of 1.3 and intercept of 51 cm/s. When fitted to a linear model, the R^2 value is 0.98 and the p-value 0.15. Error bars represent +/−1SD for both axes. Results from **Figure 11** can be used to refine the frequency analysis protocol, to deliver almost perfect correlation.

5. Discussion

This paper has presented three methods for quality assessing a complex flow phantom for medical imaging, as it operates and in real-time. The method instrumentation exploits (encoder, lasers and Doppler probe) that can collectively provide data consistent with a gold-standard method, such as Laser PIV, confirming satisfactory generation of the ring vortex to within pre-determined tolerances as listed in **Table 1**.

The instrumentation pack demonstrates its ability to characterise rings, with strong linear correlation to PIV measurements for ring speed. Configurations 1 - 5 (ring speeds 12 - 69 cm/s) report tolerances at <+/−15% from the average, reflecting previous findings from PIV datasets. In addition, piston impulse is observed to vary by <10% across all configurations. **Figure 10** demonstrates the strong correlation (R^2 = 0.99) between ring speed and CentVect in PIV datasets, indicating the importance of CentVect as a defining ring characteristic and its reliability as a QA parameter. For measurements of CentVect, data analysis is complicated by volumetric acquisition that encompasses rotational core velocities. Nonetheless, suitable analysis demonstrates strong correlation of R^2 = 0.98 across all configurations.

The addition of instrumentation doesn't disturb phantom performance, rather it increases confidence and workflow efficiency by assessment of individual rings and drastically reducing post-processing time. Given the novel design of the phantom, this is worth pursuing and could help to ease acceptance in assessing medical imaging technologies.

6. Broader Implications

Arguably, dynamic phantoms in general should incorporate adequate QA to ensure that their moving parts are functioning to specification. Confidence in the device and its performance can be heightened through varying levels of QA, as is reported in the peer reviewed literature. The most basic level is checking that an actuator/pump/motor is functioning as expected before commencing data collection [25] [26] [27]. An improvement on this is device QA performed in real-time, for instance monitoring motor speed throughout the experiment [28] [29].

The desire for real-time flow QA raises some interesting challenges. Pursuit of device QA is relatively straightforward, whereas QA of the flow directly is more difficult, particularly with complex flows. Phantoms in the literature employ reference flows ranging from laminar, parabolic flow to complex profiles incorporating eddies and recirculation zones. Simple flows are famously well-behaved and have been shown to be accurately predicted using analytical [28] [29] [30] or

CFD methods [31] [32]. These will rarely deviate from reference behaviour due to tightly constrained and simple geometries, hence non-real-time fluid predictions are sufficient, particularly when combined with real-time motor QA. Occasionally examples are presented in the literature in which real-time flow QA for a simple flow is performed [33], but this is rare and a more frequent approach is analytical or numerical predictions, or on occasion no flow QA at all [34].

Increasing the flow complexity improves physiological relevance, however the transition to disturbed flow introduces uncertainty about the intricacies of flow behaviour. Accurate analytical formulations often don't exist for such flows, and CFD simulations can be prone to errors, thus visualisation is a necessity. Often QA at this level is impractical/impossible for real-time use, because the images from scanners and the QA (e.g. PIV) of the flow can't be obtained simultaneously. Pre-collected visualisation datasets must therefore be trusted as the "ground truth" for the flow field which, as flows increase in complexity, is in danger of becoming an invalid assumption, since complex flow behaviour is rarely predictable.

Application of pre-collected visualisation data is reported in Bock *et al.* [35], whilst Meagher *et al.* [36] demonstrate an interesting approach by imaging identical phantoms simultaneously. There is no evidence of both real-time device *and* real-time flow QA beyond Vali, [28] Durand [29] and Tuncay [37], whose phantoms exhibit fairly simple flow profiles. This forms part of a trend presented in **Figure 12** and **Figure 13** below, which is that the more complex the flow, the less confidence is achieved through real-time flow QA. Phantoms suitable for a variety of modalities and applications are included in this review and

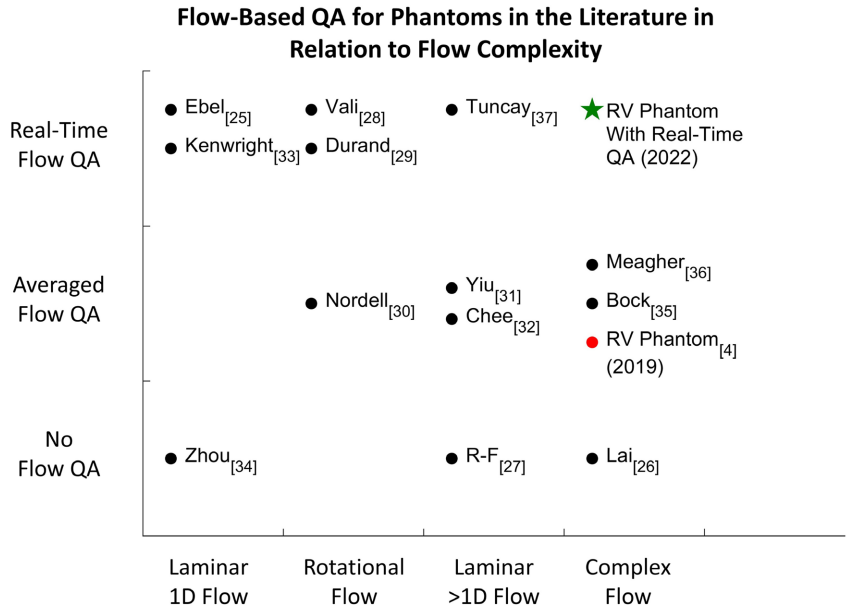

Figure 12. A qualitative graph presenting the QA procedure for flow behaviour in phantoms from the literature.

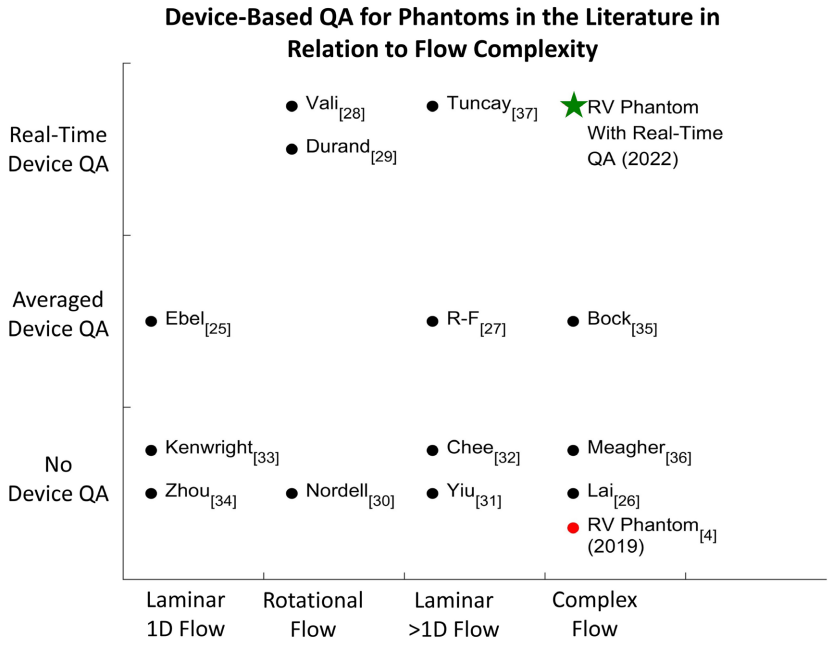

Figure 13. A qualitative graph presenting the QA procedure for device functionality in phantoms from the literature.

QA protocol is judged for measures used in regular use, not for a one-off validation exercise.

The aspirational QA standard for a dynamic, complex flow phantom would entail real-time device QA *and* flow QA. This would ordinarily be difficult, due to complex flow unpredictability and inability to produce analytical or numerical predictions. The ring vortex, however, is a complex flow that exhibits consistent behaviour and can be characterised using clear, measurable properties. Measurements collected in this paper and in previous work [4] demonstrate how well behaved the flow is, and the consistency of the device. Any abnormality in function is immediately apparent and in such cases, the ring vortex can be excluded from contributing to the flow imaging QA. **Figure 12** and **Figure 13** clarify that this is currently unique in respect of other phantoms in the literature.

In the event of a malfunction, the instrumentation pack would allow for immediate response. For example, if an incorrect setting is selected by the user resulting in a ring propagating at 70% of its desired speed, both the impulse and ring speed measurements would be below tolerances, resulting in "red" output on the user interface indicators (**Figure 6**). This would impact the CentVect value also, and the user would immediately discount the vortex and troubleshoot the problem.

Whilst each component produces meaningful information regarding the phantom and its flow, the pack as a whole (encoder, laser, probe) would be required only for specific circumstances, such as research work and assessing new technologies. A reduced requirement based on the encoder alone would suffice for regular clinical use on established technologies. This would be complemented by

regular calibration to deliver consistent performance and promote user confidence.

7. Conclusion

A novel approach to QA diagnostic flow imaging is described, incorporating real-time QA of the ring vortex flow phantom, with broader implications for complex flow phantoms. This relies on assessment of device and flow behaviour during operation, which in our case has involved three components—linear encoder (device QA), laser array (flow QA) and Doppler probe (flow QA). Together these were used to measure piston impulse, ring speed and an aspect of ring micro-flow respectively. Strong correlation was observed between reference measurements from all three methods and the Laser PIV measurements, confirming reproducibility of phantom flows within tolerances of +/−10% for rings of speeds 12 - 69 cm/s. These techniques increase confidence in phantom operation, offering a means for assessing high-resolution vector maps provided by techniques such as 4D MRI and VFI.

Acknowledgements

This work was funded by EPSRC under Grant Code 2278818. The ring vortex phantom has been manufactured using the facilities of Leeds Test Objects.

Conflicts of Interest

The authors report there are no competing interests to declare.

References

[1] Azarine, A., Garçon, P., Stansal, A., *et al.* (2019) Four-Dimensional Flow MRI: Principles and Cardiovascular Applications. *RadioGraphics*, **39**, 632-648. https://doi.org/10.1148/rg.2019180091

[2] Brandt, A.H., Olesen, J.B., Moshavegh, R., *et al.* (2021) Common Carotid Artery Volume Flow: A Comparison Study between Ultrasound Vector Flow Imaging and Phase Contrast Magnetic Resonance Imaging. *Neurology International*, **13**, 269-278. https://doi.org/10.3390/neurolint13030028

[3] Goddi, A., Bortolotto, C., Fiorina, I., *et al.* (2017) High-Frame Rate Vector Flow Imaging of the Carotid Bifurcation. *Insights into Imaging*, **8**, 319-328. https://doi.org/10.1007/s13244-017-0554-5

[4] Ambrogio, S., Walker, A., Narracott, A., *et al.* (2019) A Complex Flow Phantom for Medical Imaging: Ring Vortex Phantom Design and Technical Specification. *Journal of Medical Engineering & Technology*, **43**, 190-201. https://doi.org/10.1080/03091902.2019.1640309

[5] Ferrari, S., Ambrogio, S., Walker, A., *et al.* (2017) The Ring Vortex: Concepts for a Novel Complex Flow Phantom for Medical Imaging. *Open Journal of Medical Imaging*, **7**, 28-41. https://doi.org/10.4236/ojmi.2017.71004

[6] Arvidsson, P., Kovács, S., Töger, J., *et al.* (2016) Vortex Ring Behavior Provides the Epigenetic Blueprint for the Human Heart. *Scientific Reports*, **6**, Article No. 22021. https://doi.org/10.1038/srep22021

[7] Didden, N. (1979) On the Formation of Vortex Rings: Rolling-Up and Production of Circulation. *Journal of Applied Mathematics and Physics* (*ZAMP*), **30**, 101-116. https://doi.org/10.1007/BF01597484

[8] Maxworthy, T. (1977) Some Experimental Studies of Vortex Rings. *Journal of Fluid Mechanics*, **81**, 465-495. https://doi.org/10.1017/S0022112077002171

[9] Lim, T.T. (1989) An Experimental Study of a Vortex Ring Interacting with an Inclined Wall. *Experiments in Fluids*, **7**, 453-463. https://doi.org/10.1007/BF00187063

[10] Naitoh, T. (2002) Experimental Study of Axial Flow in a Vortex Ring. *Physics of Fluids*, **14**, 143. https://doi.org/10.1063/1.1420745

[11] Widnall, S.E., Sullivan, J.P. (1973) On the Stability of Vortex Rings. *Proceedings of the Royal Society of London A*, **332**, 335-353. https://doi.org/10.1098/rspa.1973.0029

[12] Glezer, A. and Coles, D. (1990) An Experimental Study of a Turbulent Vortex Ring. *Journal of Fluid Mechanics*, **211**, 243-283. https://doi.org/10.1017/S0022112090001562

[13] Saga, T., Hu, H., Kobayashi, T., *et al.* (2002) A Comparative Study of the PIV and LDV Measurements on a Self-Induced Sloshing Flow. *Journal of Visualization*, **3**, 145-156. https://doi.org/10.1007/BF03182407

[14] Arakeri, J.H., Das, D., Krothapalli, A., *et al.* (2004) Vortex Ring Formation at the Open End of a Shock Tube: A Particle Image Velocimetry Study. *Physics of Fluids*, **16**, 1008. https://doi.org/10.1063/1.1649339

[15] Olcay, A.B. and Krueger, P.S. (2008) Measurement of Ambient Fluid Entrainment during Laminar Vortex Ring Formation. *Experiments in Fluids*, **44**, 235-247. https://doi.org/10.1007/s00348-007-0397-9

[16] Wang, X.K., Su, B.Y., Li, Y.L., *et al.* (2019) Vortex Formation and Evolution Process in an Impulsively Starting Jet from Long Pipe. *Ocean Engineering*, **176**, 134-143. https://doi.org/10.1016/j.oceaneng.2019.02.041

[17] Weigand, A. and Gharib, M. (1997) On the Evolution of Laminar Vortex Rings. *Experiments in Fluids*, **22**, 447-457. https://doi.org/10.1007/s003480050071

[18] Murugan, T., De, S., Dora, C.L., *et al.* (2012) Numerical Simulation and PIV Study of Compressible Vortex Ring Evolution. *Shock Waves*, **22**, 69-83. https://doi.org/10.1007/s00193-011-0344-9

[19] Ma, X., Tang, Z. and Jiang, N. (2020) Visualization of Lagrangian Fluid Transport of a Vortex Ring Based on Time-Resolved PIV. *Journal of Visualization*, **23**, 559-564. https://doi.org/10.1007/s12650-020-00650-1

[20] Sun, Z.Z. and Brücker, C. (2017) Investigation of the Vortex Ring Transition Using Scanning Tomo-PIV. *Experiments in Fluids*, **58**, Article No. 36. https://doi.org/10.1007/s00348-017-2322-1

[21] Fernandez, J.J.P. and Sesterhenn, J. (2019) Axial and Radial Dynamics of Compressible Vortex Rings. *European Journal of Mechanics-B/Fluids*, **76**, 303-315. https://doi.org/10.1016/j.euromechflu.2019.03.007

[22] Sahn, D.J. and Yoganathan, A.P. (1989) Seminar on *in Vitro* Studies of Cardiac Flow and Their Applications for Clinical Doppler Echocardiography—IV. *JACC*, **12**, 1343-1376.

[23] Herr, M.D., Hogeman, C.S., Koch, D.W., *et al.* (2010) A Real-Time Device for Converting Doppler Ultrasound Audio Signals into Fluid Flow Velocity. *American Journal of Physiology Heart and Circulatory Physiology*, **298**, 1626-1632. https://doi.org/10.1152/ajpheart.00713.2009

[24] Li, Y.L., Hyun, D., Abou-Elkacem, L., Willmann, J.K., *et al.* (2016) Visualisation of Small-Diameter Vessels by Reduction of Incoherent Reverberation with Coherence Flow Power Doppler. *IEEE Transactions on Ultrasonics, Ferroelectrics, and Frequency Control*, **63**, 1878-1889. https://doi.org/10.1109/TUFFC.2016.2616112

[25] Ebel, S., Hübner, L., Köhler, B., *et al.* (2019) Validation of Two Accelerated 4D Flow Mri Sequences at 3T: A Phantom Study. *European Radiology Experimental*, **3**, Article No. 10. https://doi.org/10.1186/s41747-019-0089-2

[26] Lai, S.S., Yiu, B.Y., Poon, A.K., *et al.* (2013) Design of Anthropomorphic Flow Phantoms Based on Rapid Prototyping of Compliant Vessel Geometries. *Ultrasound in Medicine and Biology*, **39**, 1654-1664. https://doi.org/10.1016/j.ultrasmedbio.2013.03.015

[27] Raine-Fenning, N.J., Nordin, N.M., Ramnarine, K.V., *et al.* (2008) Determining the Relationship between Three-Dimensional Power Doppler Data and True Blood Flow Characteristics: An *In-Vitro* Flow Phantom Experiment. *Ultrasound in Obstetrics & Gynecology*, **32**, 540-550. https://doi.org/10.1002/uog.6110

[28] Vali, A., Schmitter, S., Ma, L., *et al.* (2020) Development of a Rotation Phantom for Phase Contrast MRI Sequence Validation and Quality Control. *Magnetic Resonance in Medicine*, **84**, 3333-3341. https://doi.org/10.1002/mrm.28343

[29] Durand, E.P., Jolivet, O., Itti, E., *et al.* (2001) Precision of Magnetic Resonance Velocity and Acceleration Measurements: Theoretical Issues and Phantom Experiments. *Journal of Magnetic Resonance Imaging*, **13**, 445-451. https://doi.org/10.1002/jmri.1064

[30] Nordell, B., Ståhlberg, F., Ericsson, A., *et al.* (1988) A Rotating Phantom for the Study of Flow Effects in MR Imaging. *Magnetic Resonance Imaging*, **6**, 695-705. https://doi.org/10.1016/0730-725X(88)90094-X

[31] Yiu, B.Y.S. and Yu, A.C.H. (2017) Spiral Flow Phantom for Ultrasound Flow Imaging Experimentation. *IEEE Transactions on Ultrasonics, Ferroelectrics, and Frequency Control*, **64**, 1840-1848. https://doi.org/10.1109/TUFFC.2017.2762860

[32] Chee, A.J.Y., Ishii, T., Yiu, B.Y.S., *et al.* (2021) Helical Toroid Phantom for 3D Flow Imaging Investigations. *Physics in Medicine & Biology*, **66**. 045029. https://doi.org/10.1088/1361-6560/abda99

[33] Kenwright, D.A., Laverick, N., Anderson, T., *et al.* (2015) Wall-Less Flow Phantom for High-Frequency Ultrasound Applications. *Ultrasound in Medicine and Biology*, **41**, 890-897. https://doi.org/10.1016/j.ultrasmedbio.2014.09.018

[34] Zhou, X.W., Kenwright, D.A., Wang, S., *et al.* (2017) Fabrication of Two Flow Phantoms for Doppler Ultrasound Imaging. *IEEE Transactions on Ultrasonics, Ferroelectrics, and Frequency Control*, **64**, 53-65. https://doi.org/10.1109/TUFFC.2016.2634919

[35] Bock, J., Töger, J., Bidhult, S., *et al.* (2019) Validation and Reproducibility of Cardiovascular 4D-Flow MRI from Two Vendors Using 2 × 2 Parallel Imaging Acceleration in Pulsatile Flow Phantom and *in vivo* with and without Respiratory Gating. *Acta Radiologica*, **60**, 327-337. https://doi.org/10.1177/0284185118784981

[36] Meagher, S., Poepping, T.L., Ramnarine, K.V., *et al.* (2007) Anatomical Flow Phantoms of the Nonplanar Carotid Bifurcation, Part II: Experimental Validation with Doppler Ultrasound. *Ultrasound in Medicine and Biology*, **33**, 303-310. https://doi.org/10.1016/j.ultrasmedbio.2006.08.004

[37] Tuncay, V., Zijlstra, J., Oudkerk, M., *et al.* (2020) Design, Implementation, and Validation of a Pulsatile Heart Phantom Pump. *Journal of Digital Imaging*, **33**, 1301-1305. https://doi.org/10.1007/s10278-020-00375-5

Appendix

Derivation of Impulse delivered by piston:

T—Piston Pulse Time Duration

R_0—Piston Radius

L—Piston Displacement

r—Orifice Radius

ρ—Density of water

Fluid Slug Volume = $V = \pi R_0^2 L$

Jet Length = $L_s = \dfrac{V}{\pi r^2} = \dfrac{R_0^2 L}{r^2}$

Jet Speed = $S = \dfrac{L_s}{T} = \dfrac{R_0^2 L}{r^2 T}$

Jet Energy = $E = \dfrac{1}{2}mv^2 = \dfrac{1}{2}\rho V S^2 = \dfrac{1}{2}\dfrac{R_0^6 L^3 \rho\pi}{r^4 T^2}$

Force of Jet = *Energy/Distance* = $\dfrac{E}{L_s} = \dfrac{1}{2}\dfrac{R_0^6 L^3 \rho\pi r^2}{r^4 T^2 R_0^2 L}$

Jet Impulse = *Force* * *Time* = $\dfrac{1}{2}\dfrac{R_0^4 L^2 \rho\pi}{r^2 T}$